SCIENCE CHINA
Information Sciences

• RESEARCH PAPER •

October 2024, Vol. 67, Iss. 10, 202205:1–202205:15
https://doi.org/10.1007/s11432-023-4094-4

# State and parameter identification of linearized water wave equation via adjoint method

Yang YU[1], Cheng-Zhong XU[2*], Hai-Long PEI[3] & Jinpeng YU[1*]

[1]*School of Automation, Qingdao University, Qingdao* 266071*, China;*
[2]*LAGEP, Batiment CPE, University Claude Bernard-Lyon 1, Villeurbanne Cedex* 69622*, France;*
[3]*School of Automation Science and Engineering, Key Laboratory of Autonomous Systems and Networked Control, Ministry of Education, Guangdong Engineering Technology Research Center of Unmanned Aerial Vehicle System, South China University of Technology, Guangzhou* 510641*, China*

Received 31 May 2023/Revised 30 October 2023/Accepted 5 January 2024/Published online 13 September 2024

**Abstract** In this paper, we focus on the state and parameter identification problem of a hydrodynamical system. This system is modeled as a linearized water wave equation (LWWE), a hyperbolic state-space model coupled with a Laplace equation. We assume that the wave elevation at two distinct points is the only measurement of water waves. We show that the state and water depth can be reconstructed from this point measurement records. The identification problem is recast as an optimization problem over an infinite-dimensional space. We propose the adjoint method-based identification algorithm to generate an estimated state and water depth. We then performed a numerical simulation to show the effectiveness of our designed algorithm by comparing it with existing studies.

**Keywords** linearized water wave equation (LWWE), point observation, state estimation, parameter identification, adjoint method, numerical simulation

## 1 Introduction

### 1.1 Linearized water wave equation

We study the parameter identification and state estimation for a linearized water wave equation (LWWE) in a bounded rectangular domain $\Omega = \{(x, y) \in (0, L) \times (-h, 0)\}$, where $L$ and $h > 0$ denote the container length and water depth, respectively. Figure 1 shows a diagram of the domain $\Omega$, where $\eta = \eta(x, t)$ is the wave elevation at position $x$ and time $t$. To write the LWWE, we assume that the water and water waves in $\Omega$ are incompressible, inviscid, and irrotational, and we also neglect the surface pressure. The irrotational assumption implies that there exists a multivariable function, denoted by $\phi = \phi(x, y, t)$ and named as velocity potential, such that the velocity field of water waves, denoted by $u$, is equal to the gradient of $\phi$, i.e., $u = \nabla\phi = (\phi_x, \phi_y)^{\mathrm{T}}$, where $\phi_x$ and $\phi_y$ denote the partial derivative of $\phi$ with respect to $x$ and $y$, respectively. According to the conservation of mass law, at each time $t$, the velocity potential $\phi$ is a harmonic function, i.e.,

$$\frac{\partial^2\phi}{\partial x^2}(x, y, t) + \frac{\partial^2\phi}{\partial y^2}(x, y, t) = 0, \quad (x, y) \in \Omega. \tag{1}$$

On the lateral boundary ($x = 0$ and $x = L$) and on the flat bottom ($y = -h$), the velocity satisfies the solid wall condition so that

$$\begin{aligned} &\frac{\partial\phi}{\partial x}(0, y, t) = \frac{\partial\phi}{\partial x}(L, y, t) = 0, \quad y \in (-h, 0),\ t > 0, \\ &\frac{\partial\phi}{\partial y}(x, -h, t) = 0, \qquad\qquad\qquad\quad x \in (0, L),\ t > 0. \end{aligned} \tag{2}$$

* Corresponding author (email: cheng-zhong.xu@univ-lyon1.fr, yjp1109@hotmail.com)

 

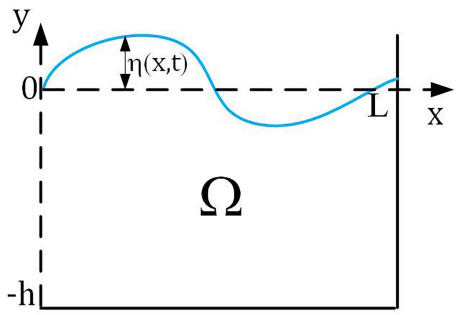


**Figure 1** (Color online) Schematic view of the water waves in the domain Ω.

Two boundary conditions govern the velocity potential on the free surface ($y = 0$):

$$\begin{aligned} &\frac{\partial \phi}{\partial t}(x,0,t) = -g\eta(x,t), \qquad x \in (0,L), t > 0, \\ &\frac{\partial \eta}{\partial t}(x,t) = \frac{\partial \phi}{\partial y}(x,0,t), \qquad x \in (0,L), t > 0. \end{aligned} \tag{3}$$

The first equation of (3) is an approximated model obtained by tangent linearization of the Bernoulli equation around the equilibrium point ($y = 0$) (where $g$ is Newton's constant of gravitation). Meanwhile, the second equation denotes that the vertical component of the velocity field on the surface of water waves ($\phi_y(x,0,t)$) is just the wave speed. For the water wave equation and its linearization version (1)–(3), refer to the book of Dean and Dalrymple [1], Whitham [2], and Lannes [3].

Regarding the LWWE, we state that it is not easy to see from Figure 1 that the water domain is time-invariant, and one may misunderstand it as a time-varying domain $\{(x,y) \in (0,L) \times (-h, \eta(x,t))\}$. The linearization process transforms the upper boundary condition from $y = \eta(x,t)$ to $y = 0$. We also state that the solution of the LWWE consists of not only the velocity potential $\phi$ but also the wave elevation $\eta$.

### 1.2 Research motivation

Well-known ships sailing near the shoreline must predict the hydrological characteristics in front of the channel in real time to make navigation decisions. Here, hydrological features include the unmeasurable underwater flow velocity field and the seabed topography inversion. Ref. [4] used the least square method to estimate the amplitude of wave elevation. However, such an estimation is insufficient, especially as Ref. [4] has assumed that the water depth is known a priori. Moreover, Refs. [5, 6] took the nonlinear water wave equation as the mathematical model of water waves and analyzed the identifiability of water depth. They proved that the water depth can be identified if the distributed states of the water wave system are measurable. However, as indicated by Vasan and Deconinck in [6], we should be aware of the difficulty in measuring the distributed velocity potential of water waves. Therefore, we aim to study the LWWE as the mathematical model of water waves. We then analyze the identifiability of both the water depth and the state of the water wave system by measuring the surface wave elevation at two distinct points. Finally, we will propose a system identification algorithm that simultaneously estimates the water depth and the distributed states of water waves by using point water elevation measurements only.

### 1.3 Literature review on control and observation of LWWE

To the best of our knowledge, very few articles deal with the application of control and observation theory to the LWWE (1)–(3). Russel and Reid [7] published the first result regarding the controllability and stabilizability of LWWE with infinite water depth. Mottelet [8] then conducted different studies on the controllability of LWWE with finite depth. Recently, Su et al. [9] have studied the strong stabilizability of the LWWE. Alazard [10] also studied the state observability of the nonlinear water wave equation. At the same time, we have studied the state observability of the periodical LWWE in [11], where we have designed an infinite-dimensional observer to estimate the state of the linear water waves. The result of [11] has been extended in [12], in which the distributed observation of wave elevation has been updated as a point observation. However, few research articles focused on water depth identification based on the

LWWE. In [13], we showed that periodical LWWE can be used to estimate the water depth and velocity potential by measuring the distributed wave elevation. The classical gradient descent method (GDM) was employed to estimate them.

In this paper, we expect to improve the identification performance for the state and parameters of water waves by applying the adjoint method. This approach was initially used to estimate the initial values of the overland flow model (see [14]). The technical route of the adjoint method involves using the Lagrange multiplier method to define a cost function that can characterize the accuracy of identification and then constructing the adjoint equation associated with the LWWE by computing the first variation of the cost function. The direction of reducing the cost function can be determined by solving the adjoint equation. Finally, a GDM is used to update the parameters iteratively so that the parameters of water waves converge to the true values. This method has been successfully used to estimate the parameters of the wave equation (see [15]) and to estimate the initial values of the 1D hyperbolic equation [16]. Moreover, Ref. [15] has tested the effectiveness of the adjoint method with experimental data. Compared with the classical GDM (see [17] for a general presentation of GDM), the adjoint method requires the analytical solution of the LWWE to obtain the cost functional gradient. Therefore, the adjoint method-based parameter identification approach to water waves is more suitable for implementation in practice and offers a generalization to other cases.

### 1.4 Contribution of the paper

It should be noted that the boundary observation of the LWWE poses a severe challenge. One challenge is that the LWWE has a two-dimensional geometric spatial domain, but the observation is restricted to some boundary points. This necessitates the propagation of state information across the entire spatial domain to these specific points. This phenomenon occurs in other partial differential equation (PDE) systems, such as the two-dimensional wave equation with boundary observations (see [18]). On the other hand, the two-dimensional heat equation still has an unlimited propagating velocity (see [19]).

Another challenge is that the LWWE is a PDE-PDE coupling system as dynamical state equations are coupled with a statical Laplace equation (see Section 2). The dynamic models considered in [14–16] are composed of only a single PDE. Therefore, how to apply the Lagrange multiplier method to define the cost functional for the LWWE and compute its Frechet gradient constitutes an algorithmic challenge.

The contribution of this paper is twofold. First, it shows the identifiability of the LWWE from the measurement of two-point wave elevations. Second, it designs an identification algorithm to simultaneously estimate both the water depth and the distributed states of the LWWE.

The rest part of the paper is organized as follows. We present some preliminaries of the LWWE in Section 2. We present the proof of identifiability of the system in Section 3. We present our designed identification algorithm in Section 4. We give some numerical simulations to illustrate the performance of our developed algorithm in Section 5. We provide the conclusion in Section 6.

### 1.5 Notation

Throughout the paper, $\mathbb{N}$ denotes the set of natural numbers starting with 1. Let $C^\infty[0,L]$ be the set of infinitely differentiable functions defined on $[0,L]$. We then define $C_0^\infty[0,L]$ as

$$C_0^\infty[0,L]=\left\{f\in C^\infty[0,L]\,\middle|\,\int_0^L f(x)\mathrm{d}x=0\right\}.$$

$L^2(0,L)$ denotes the set of square-integrable functions defined on $(0,L)$ equipped with the usual norm $\|\cdot\|_{L^2}$. Then $L_0^2(0,L)$ is the completion of $C_0^\infty[0,L]$ with respect to the $L^2$-norm. Furthermore, let $H^1(0,L)$ denote the first-order Sobolev space equipped with the norm $\|f\|_{H^1}^2=\|f\|_{L^2}^2+\|f'\|_{L^2}^2,\ \forall f\in H^1(0,L)$. Furthermore, $H_0^1(0,L)$ is the completion of $C_0^\infty[0,L]$ with respect to the $H^1$ norm. Consider a function $f\in C^\infty[0,L]$ written as

$$f(x)=\sum_{m=1}^{\infty}\sqrt{\frac{2}{L}}a_m\cos(k_m x),$$

where $k_m=m\pi/L, m\in\mathbb{N}$. We define an $H^{1/2}$ norm as

$$\|f\|_{H^{1/2}}^2=\sum_{m=1}^{\infty}\left(\frac{k_m}{g}\right)\tanh(k_m h)a_m^2. \tag{4}$$

The fractional-order Sobolev space $H_0^{1/2}(0,L)$ can then be regarded as the completion of $C_0^\infty[0,L]$ with respect to the $H^{1/2}$ norm.

## 2 Preliminaries

In this section, we present some preliminaries regarding the well posedness of LWWE (1)–(3). According to the Craig-Sulem-Zakharov formulation (see [20,21]), we can transform the dynamical boundary conditions (3) into an equivalent state-space representation model by defining the state $\xi(x,t)$ as the velocity potential on the surface, i.e., $\xi(x,t)=\phi(x,0,t)$. This implies that $\xi_t(x,t)=\phi_t(x,0,t)$. The state-space model of the LWWE is then governed by

$$\begin{aligned}
&\xi_t(x,t)=-g\eta(x,t), \quad x\in(0,L),\ t>0,\\
&\eta_t(x,t)=G\xi(x,t), \quad x\in(0,L),\ t>0,\\
&\xi(x,0)=\xi^0(x),\ \ \eta(x,0)=\eta^0(x),\\
&y_{\mathrm{out},1}(t)=\eta(0,t),\quad y_{\mathrm{out},2}(t)=\eta\left(\frac{L}{\pi},t\right),\ \ t\in[0,\infty),
\end{aligned}\tag{5}$$

where $(\xi^0,\eta^0)$ is the initial condition of the dynamical system, and $y_{\mathrm{out},i}(t)$ is the measurement output $(i=1,2)$. We assume that the wave elevation at $x=0$ and $x=L/\pi$ for all $t\geqslant 0$ is measurable. Notice that $G$ is a linear operator named the Dirichlet-Neumann operator, which maps each $\xi(x,t)$ to $\phi_y(x,0,t)$, with $\phi(x,y,t)$ being the solution of the following Laplace PDE:

$$\begin{cases}
\Delta\phi(x,y,t)=0, & (x,y)\in\Omega, t>0,\\
\phi_x(0,y,t)=\phi_x(L,y,t)=0, & y\in(-h,0), t>0,\\
\phi_y(x,-h,t)=0, & x\in(0,L), t>0,\\
\phi(x,0,t)=\xi(x,t), & x\in(0,L), t>0.
\end{cases}\tag{6}$$

More simply, let $\phi_y(x,0,t)=G\xi(x,t)$.

**Remark 1.** Physically, infrared LiDAR can measure the water wave elevation. We refer the interested reader to [22], where the authors have used high-precision and high-density infrared LiDAR to observe the water wave elevation.

Our previous work (see [11,13]) proved that the Laplace equation (6) is well posed. Precisely, once $\xi\in C_0^\infty[0,L]$, such that

$$\xi(x)=\sum_{m=1}^{\infty}\sqrt{\frac{2}{L}}a_m\cos(k_m x)\tag{7}$$

with $(k_m^n a_m)\in\ell^2$, $\forall n\in\mathbb{N}$, then the velocity potential $\phi\in C_0^\infty(\overline{\Omega})$ can be obtained via the separation of variables method and uniquely expressed as

$$\phi(x,y)=\sum_{m=1}^{\infty}\sqrt{\frac{2}{L}}a_m\cos(k_m x)\frac{\cosh(k_m(y+h))}{\cosh(k_m h)},\tag{8}$$

where $k_m=m\pi/L$ with $m\in\mathbb{N}$. Moreover, if $\xi\in C_0^\infty[0,L]$ is written as (7), then $G(\xi)$ is written as

$$G(\xi)=\sum_{m=1}^{\infty}\sqrt{\frac{2}{L}}a_m k_m\tanh(k_m h)\cos(k_m x).\tag{9}$$

Here, the sequence $(a_m)$ satisfies $(a_m k_m^n)\in\ell^2$, $\forall n\in\mathbb{N}$.

The following lemma, whose proof can be found in [12], describes some properties of the operator $G$.

**Lemma 1.** The linear operator $G: H_0^1(0,L)\to L_0^2(0,L)$ is bounded and invertible. The same operator defined as $G: D(G)\subset L_0^2(0,L)\to L_0^2(0,L)$ is unbounded, self-adjoint, and positive definite with compact resolvents.

The term "Dirichlet-Neumann" comes from the fact that $G$ maps the Dirichlet boundary condition of the Laplace equation on the upper boundary of $\Omega$ onto a Neumann boundary condition on the same boundary. From this, we claim that $G^{-1}$ is a "Neumann-Dirichlet" operator. In other words, for a given function $f \in L_0^2(0,L)$, $G^{-1}(f)$ is the solution $u$ of the following Laplace PDE evaluated on $y=0$, or, more simply, $u(x,0) = G^{-1}(f)(x)$:

$$\begin{cases} \Delta u(x,y) = 0, & (x,y) \in \Omega, \\ u_x(0,y) = u_x(L,y) = 0, & y \in (-h,0), \\ u_y(x,-h) = 0, & x \in (0,L), \\ u_y(x,0) = f(x), & x \in (0,L). \end{cases} \tag{10}$$

The proof sketch of this claim is first to substitute

$$f(x) = \sum_{m=1}^{\infty} \sqrt{\frac{2}{L}} a_m \cos(k_m x) \in C_0^{\infty}[0,L]$$

into (10) and then use the separation of variables method similar to that in [13, Theorem 2.1] to determine the solution of the Laplace PDE as follows:

$$u(x,y) = \sum_{m=1}^{\infty} \sqrt{\frac{2}{L}} \frac{a_m}{k_m \sinh(k_m h)} \cos(k_m x) \cosh(k_m (y+h)),$$

with $u \in C^{\infty}(\overline{\Omega})$. Finally, evaluating $u$ at the upper boundary at $y=0$, we obtain

$$G^{-1}(f)(x) = u(x,0) = \sqrt{\frac{2}{L}} \sum_{m=1}^{\infty} \left( \frac{a_m}{k_m \tanh(k_m h)} \right) \cos(k_m x).$$

Notice that the spectrum of $G$ being discrete is constituted of eigenvalues only, i.e.,

$$\sigma(G) = \{\lambda_m = k_m \tanh(k_m h) \mid m \in \mathbb{N}\},$$

where $k_m = m\pi/L$, $\forall m \in \mathbb{N}$ and the corresponding eigenvector $e_m$ is $e_m(x) = \cos(k_m x)$, $\forall m \in \mathbb{N}$.

Now, let us consider the well posedness of the dynamical system (5). Consider the system in the state space $X = H_0^1(0,L) \times H_0^{1/2}(0,L)$ equipped with the norm

$$\left\| \begin{pmatrix} f \\ g \end{pmatrix} \right\|_X^2 = \|G(f)\|_{L^2}^2 + \|G^{\frac{1}{2}}(g)\|_{L^2}^2, \ \ \forall \begin{pmatrix} f \\ g \end{pmatrix} \in X.$$

By (4) and (9), it is clear that the following holds:

$$\|f\|_{H^{\frac{1}{2}}}^2 = \left\| \frac{G^{\frac{1}{2}} f}{\sqrt{g}} \right\|_{L^2}^2.$$

Define the operator $A : D(A) \subset X \to X$ as

$$\begin{aligned} A \begin{pmatrix} u \\ v \end{pmatrix} &= \begin{pmatrix} -gv \\ G(u) \end{pmatrix}, \\ D(A) &= H_0^{\frac{3}{2}}(0,L) \times H_0^1(0,L). \end{aligned} \tag{11}$$

Refs. [11, 13] proved that $A$ is the generator of a unitary $C_0$-semigroup $(\mathbb{T}_t)_{t \geqslant 0}$ on $X$. This implies that if the initial condition of (5) is $(\xi^0, \eta^0) \in X$, then the solution $(\xi(\cdot,t), \eta(\cdot,t))^{\mathrm{T}} \in C([0,\infty), X)$, and the unique solution is written as

$$\begin{pmatrix} \xi(\cdot,t) \\ \eta(\cdot,t) \end{pmatrix} = \mathbb{T}_t \begin{pmatrix} \xi^0(\cdot) \\ \eta^0(\cdot) \end{pmatrix}, \ \ t \geqslant 0.$$

Furthermore, some simple and straightforward computations allow us to determine the analytical solution of the LWWE. First, it is easy to check that

$$\left(\sqrt{\frac{2}{L}}\frac{g}{\omega_m}\cos(k_m x)\right)_{m\in\mathbb{N}},\ \left(\sqrt{\frac{2}{L}}\cos(k_m x)\right)_{m\in\mathbb{N}}$$

form an orthonormal basis of $H_0^{1/2}(0,L)$ and $L_0^2(0,L)$, respectively, where $k_m = m\pi/L$ and $\omega_m = \sqrt{gk_m\tanh(k_m h)}$. We then assume that the solution of the LWWE is

$$\begin{aligned}\xi(x,t) &= \sum_{m=1}^{\infty}\sqrt{\frac{2}{L}}\frac{g}{\omega_m}A_m(t)\cos(k_m x),\\ \eta(x,t) &= \sum_{m=1}^{\infty}\sqrt{\frac{2}{L}}B_m(t)\cos(k_m x).\end{aligned}\tag{12}$$

Substituting them into the LWWE (5), we see that the Fourier coefficients $A_m(t)$ and $B_m(t)$ must satisfy the following ordinary differential equations (ODEs):

$$\begin{aligned}\dot{A}_m(t) &= -\omega_m B_m(t),\\ \dot{B}_m(t) &= \omega_m A_m(t).\end{aligned}$$

It is easy to solve these ODEs. If let $A_m(0)$ and $B_m(0)$ denote the initial values of $A_m(t)$ and $B_m(t)$, respectively, then

$$\begin{aligned}A_m(t) &= A_m(0)\cos(\omega_m t) - B_m(0)\sin(\omega_m t),\\ B_m(t) &= A_m(0)\sin(\omega_m t) + B_m(0)\cos(\omega_m t),\end{aligned}\tag{13}$$

where $A_m(0)$ and $B_m(0)$ are uniquely determined by the initial conditions $(\xi^0,\eta^0)$ as follows:

$$\begin{aligned}A_m(0) &= \left\langle \xi^0(x), \sqrt{\frac{2}{L}}\frac{g}{\omega_m}\cos(k_m x)\right\rangle_{H^{1/2}},\\ B_m(0) &= \left\langle \eta^0(x), \sqrt{\frac{2}{L}}\cos(k_m x)\right\rangle_{L^2}.\end{aligned}$$

## 3 Identifiability analysis

Identifiability is a fundamental question arising in inverse problems. Roughly speaking, if the measured data contain sufficient information for the unknown quantity to be uniquely determined, then we say that the unknown quantity is identifiable from the prescribed observation.

The state space is the Hilbert space $X = H_0^1(0,L)\times H_0^{\frac{1}{2}}(0,L)$. We will need another smaller Hilbert space $X_\epsilon = H_0^{1+\epsilon}(0,L)\times H_0^{1/2+\epsilon}(0,L)$ that is dense in $X$ for any $\epsilon>0$. Notice that $X_\epsilon \supset \mathcal{D}(A)$, $\forall\epsilon>0$ is small enough. Let $p = (h,\xi^0,\eta^0)^{\mathrm{T}}$ denote the vector of parameters to be identified. We assume $h>0$ and that two-point water wave elevations are measured:

$$y_1(t) = \eta(0,t),\ \ y_2(t) = \eta(L/\pi,t).$$

We want to identify the parameter vector $p$ from the measurement $(y_1(t),y_2(t))$.

From Section 2, once the initial values of the dynamical system (5) are written as

$$\begin{aligned}\xi^0(x) &= \sqrt{\frac{2}{L}}\sum_{m=1}^{\infty}\frac{g}{\omega_m}a_m\cos(k_m x),\\ \eta^0(x) &= \sqrt{\frac{2}{L}}\sum_{m=1}^{\infty}b_m\cos(k_m x),\end{aligned}\tag{14}$$

where $k_m = m\pi/L$ and $\omega_m = \sqrt{gk_m \tanh(k_m h)}$, then the water wave elevation measurements are uniquely determined as

$$y_1(t) = \eta(0,t) = \sqrt{\frac{2}{L}} \sum_{m=1}^{\infty} [a_m \sin(\omega_m t) + b_m \cos(\omega_m t)], \tag{15}$$

$$y_2(t) = \eta(L/\pi,t) = \sqrt{\frac{2}{L}} \sum_{m=1}^{\infty} [a_m \sin(\omega_m t) + b_m \cos(\omega_m t)] \cos(m). \tag{16}$$

Theorem 1 gives the identifiability result.

**Theorem 1.** The parameter vector $p$ is identifiable from all nonzero initial conditions $(\xi^0, \eta^0) \in X_\epsilon$ for an $\epsilon > 0$. More precisely, let $p = (h, \xi^0, \eta^0)^{\mathrm{T}}$ and $\tilde{p} = (\tilde{h}, \tilde{\xi}^0, \tilde{\eta}^0)^{\mathrm{T}}$ be two vectors of parameters, and let the corresponding measurement outputs be $y_i(t)$ and $\tilde{y}_i(t)$, respectively, where $t \geqslant 0$ and $i = 1, 2$. Then $y_i(t) = \tilde{y}_i(t)$, $\forall t \in [0, \infty)$ and $\forall i = 1, 2$ implies that $p = \tilde{p}$.

*Proof.* Notice that the initial condition $(\xi^0, \eta^0) \in X_\epsilon$ guarantees that series (15) and (16) converge absolutely and uniformly on $[0, \infty)$. This fact is used to perform the subsequent limit inversion.

Similarly, given $\tilde{p}$, we write

$$\begin{aligned} \tilde{\xi}^0(x) &= \sqrt{\frac{2}{L}} \sum_{m=1}^{\infty} \frac{g}{\tilde{\omega}_m} \tilde{a}_m \cos(k_m x), \\ \tilde{\eta}^0(x) &= \sqrt{\frac{2}{L}} \sum_{m=1}^{\infty} \tilde{b}_m \cos(k_m x), \end{aligned} \tag{17}$$

where $k_m = m\pi/L$ and $\tilde{\omega}_m = \sqrt{gk_m \tanh(k_m \tilde{h})}$, and

$$\tilde{y}_1(t) = \tilde{\eta}(0,t) = \sqrt{\frac{2}{L}} \sum_{m=1}^{\infty} [\tilde{a}_m \sin(\omega_m t) + \tilde{b}_m \cos(\tilde{\omega}_m t)], \tag{18}$$

$$\tilde{y}_2(t) = \tilde{\eta}(L/\pi,t) = \sqrt{\frac{2}{L}} \sum_{m=1}^{\infty} [\tilde{a}_m \sin(\tilde{\omega}_m t) + \tilde{b}_m \cos(\tilde{\omega}_m t)] \cos(m). \tag{19}$$

Assume that $y_i(t) = \tilde{y}_i(t)$, $\forall\, i = 1, 2$ on $[0, \infty)$. As the initial condition is nonzero, i.e., $(\xi^0, \eta^0) \neq (0,\ 0)$, there exists at least some integer $l > 0$ such that $a_l \neq 0$ (or, similarly $b_l \neq 0$). We can then easily check that the following holds:

$$\lim_{T\to\infty} \frac{1}{T} \int_0^T y_i(t) \sin(\omega_l t) \mathrm{d}t = \lim_{T\to\infty} \frac{1}{T} \int_0^T \tilde{y}_i(t) \sin(\omega_l t) \mathrm{d}t,\ i = 1, 2, \tag{20}$$

$$\lim_{T\to\infty} \frac{1}{T} \int_0^T \sin(\omega_m t) \sin(\omega_l t) \mathrm{d}t = \begin{cases} 0, & m \neq l, \\ \frac{1}{2}, & m = l, \end{cases} \tag{21}$$

and

$$\lim_{T\to\infty} \frac{1}{T} \int_0^T \cos(\omega_m t) \sin(\omega_l t) \mathrm{d}t = 0 \ \ \forall m \in \mathbb{N}. \tag{22}$$

On the other hand, there exists necessarily some integer $s > 0$ such that $\tilde{\omega}_s = \omega_l$. Otherwise, similarly to (21) and (22) and by (20), we get the contradiction that $a_l = 0$. By absolutely uniform convergence of the series from (20) and for $i = 1$, it follows that

$$a_l = \tilde{a}_s,\ \omega_l = \tilde{\omega}_s \tag{23}$$

and for $i = 2$,

$$\cos(m)\, a_l = \cos(s)\, \tilde{a}_s. \tag{24}$$

Since both $s$ and $l$ are positive integers, it is implied from the above (23) and (24) that $s = l$. Moreover, $\omega_l = \tilde{\omega}_l$ and $a_l = \tilde{a}_l$. From the definition of $\omega_l$ and $\tilde{\omega}_l$, we get $h = \tilde{h}$. The last equality immediately implies that $\omega_m = \tilde{\omega}_m$, $\forall m \in \mathbb{N}$. Substituting $l$ by arbitrary $m$ in (20) and then $\sin(\omega_l t)$ by $\cos(\omega_m t)$ allows us to obtain $a_m = \tilde{a}_m$ and $b_m = \tilde{b}_m$, $\forall m \in \mathbb{N}$. By (14) and (17), we prove that $(\xi^0, \eta^0) = (\tilde{\xi}^0, \tilde{\eta}^0)$. Hence $p = \tilde{p}$.

**Remark 2.** We claim that the unknown parameter $p = (h, \xi^0, \eta^0)^{\mathrm{T}}$ cannot be identified if the measured data of the water wave system is $\eta(x^*, t)$, where $x^*$ is an arbitrary point in $[0,\ L]$. In other words, we cannot identify the parameters with an arbitrary point measurement. Indeed, from (14), we can write $\eta(x^*, t)$ as follows:

$$\eta(x^*,t)=\sqrt{\frac{2}{L}}\sum_{m=1}^{\infty}[\tilde{a}_m\sin(\omega_m t)+\tilde{b}_m\cos(\omega_m t)], \tag{25}$$

where $\tilde{a}_m = a_m\cos(k_m x^*)$ and $\tilde{b}_m = b_m\cos(k_m x^*)$. Take $x^* = L/2$, $a_1 = b_1 = 1$, and $a_m = b_m = 0$ $\forall m \neq 1$. It is clear that $y(t) = \eta(x^*, t) = 0$, $\forall t \in [0, \infty)$. However, $(\xi^0, \eta^0) \neq (0, 0)$. Hence, the parameter vector $p$ is not identifiable from $(h, \xi^0, 0)$.

## 4 Identification algorithm

In this section, we provide an algorithm of estimation that can simultaneously recover the water depth and the state variables from the measurement of water wave elevation at $x = 0$ and $x = \frac{L}{\pi}$. Note that the dependence of domain $\Omega$ on water depth gives great inconvenience in computing the cost functional differential. To solve this problem, we transform the water domain into a depth-independent domain $\tilde{\Omega} = \{(x, \tilde{y}) \in (0, L) \times (-1, 0)\}$ by introducing a dimensionless variable $\tilde{y} = y/h$. In the new coordinate system $(x, \tilde{y})$, the governing equations of linear water waves and the related boundary conditions are transformed into the following:

$$\begin{aligned}
&\xi_t(x,t) = -g\eta(x,t), && x \in (0,L), t>0,\\
&\eta_t(x,t) = HG(\xi(x,t)), && x \in (0,L), t>0,\\
&\xi(x,0) = \xi^0(x), && \eta(x,0) = \eta^0(x),
\end{aligned} \tag{26}$$

where $H = h^{-1}$ is the inverse of water depth and $G$ is the abovementioned Dirichlet-Neumann operator defined as $G : \xi \mapsto \phi_y(x, 0, t)$ with $\phi$ being the solution of the following elliptic PDE:

$$\begin{aligned}
&\phi_{xx}(x,\tilde{y},t)+H^2\phi_{\tilde{y}\tilde{y}}(x,\tilde{y},t)=0, && (x,\tilde{y}) \in \tilde{\Omega}, t>0,\\
&\phi_x(0,\tilde{y},t)=\phi_x(L,\tilde{y},t)=0, && \tilde{y} \in (-1,0), t>0,\\
&H\phi_{\tilde{y}}(x,-1,t) = 0, && x \in (0,L), t>0,\\
&\phi(x,0,t) = \xi(x,t), && x \in (0,L), t>0.
\end{aligned} \tag{27}$$

Thus, the estimation of water depth is equivalent to the estimation of $H$. Hereafter, we will continue to use $y$ to represent the vertical axis $\tilde{y}$.

The vector of parameters to be identified is denoted by $p = (H, \xi^0, \eta^0)^{\mathrm{T}}$, which is involved in the parameter space $\mathbb{R}^+ \times H_0^{\frac{1}{2}}(0, L) \times L_0^2(0, L)$ equipped with the scalar product

$$\langle p, \hat{p}\rangle = H\hat{H} + \langle \xi^0, \hat{\xi}^0\rangle_{H^{1/2}} + \langle \eta^0, \hat{\eta}^0\rangle_{L^2}. \tag{28}$$

The purpose of identification is to determine the optimal parameter $p$ to minimize the following cost functional:

$$\begin{aligned}
J(p) = \frac{1}{2}\int_0^T \left\{ \left[\int_0^L D(x)\eta(x,t)\mathrm{d}x - \hat{\eta}(0,t)\right]^2 + \left[\int_0^L D\left(x-\frac{L}{\pi}\right)\eta(x,t)\mathrm{d}x - \hat{\eta}\left(\frac{L}{\pi},t\right)\right]^2 \right\}\mathrm{d}t\\
+ \frac{1}{2}\int_0^L \epsilon_1\left[\xi^0(x)-\xi_F^0(x)\right]^2 + \epsilon_2\left[\eta^0(x)-\eta_F^0(x)\right]^2\mathrm{d}x,
\end{aligned} \tag{29}$$

where $T$ is the final time of observation, $\hat{\eta}(0, t)$ and $\hat{\eta}(\frac{L}{\pi}, t)$ are the measurement of the dynamical system, $\xi_F^0$ and $\eta_F^0$ are the first guessed value of initial condition, and $\epsilon_1$ and $\epsilon_2$ are two weighting factors applied to the first guessing term to calibrate the estimated and guessed values and adjust the scale of the objective function. $D(x)$ is the Delta-Dirac function defined by $D(x) = 0$ for $x \neq 0$ and $\int_{-\infty}^{+\infty} D(x)\mathrm{d}x = 1$.

It should be noted that the optimal state and parameter values must minimize the cost functional in (29) and also satisfy the system equation (26) and (27). This constraint and the continuity of the first partial derivative of both system dynamics and cost function make it possible to use the Lagrange multiplier to combine the system equation and cost function into only one new cost functional $\mathcal{L}(\lambda, p)$, i.e., the Lagrangian functional, written $\mathcal{L}$ in abbreviation, as follows:

$$\begin{aligned}\mathcal{L} = J+\int_0^T\int_0^L\int_{-1}^0 \lambda_1(x,y,t)\left(\phi_{xx}+H^2\phi_{yy}\right)\mathrm{d}y\mathrm{d}x\mathrm{d}t+\int_0^T\int_0^L \lambda_2(x,t)\left[\xi_t(x,t)+g\eta(x,t)\right]\mathrm{d}x\mathrm{d}t\\ +\int_0^T\int_0^L \lambda_3(x,t)\left[\eta_t(x,t)-HG(\xi(x,t))\right]\mathrm{d}x\mathrm{d}t.\end{aligned} \tag{30}$$

The terms $\lambda_1, \lambda_2, \lambda_3$ are the Lagrange multipliers corresponding to the system equation (26) and (27).

Under suitable conditions, the following result provides an expression of the cost functional derivative.

**Theorem 2.** Let $p = (H, \xi^0, \eta^0)$. The differential of $\mathcal{L}$ defined in (30) with respect to $p$ is given by

$$\delta\mathcal{L} = \langle \mathrm{d}\mathcal{L}, \delta p\rangle, \tag{31}$$

where

$$\mathrm{d}\mathcal{L} = \begin{bmatrix} \int_0^T\int_0^L\int_{-1}^0 2H\lambda_1\phi_{yy}\mathrm{d}y\mathrm{d}x\mathrm{d}t - \int_0^T\int_0^L \lambda_3 G(\xi)\mathrm{d}x\mathrm{d}t \\ G^{-1}[g\epsilon_1(\xi^0-\xi_F^0)-g\lambda_2(x,0)] \\ \epsilon[\eta^0-\eta_F^0]-\lambda_3(x,0)\end{bmatrix} \tag{32}$$

is the cost functional derivative and belongs to the parameter space defined in (28). $\lambda_1, \lambda_2$, and $\lambda_3$ are the unique solutions of the following adjoint equations:

$$\begin{cases}\lambda_{2t}(x,t) = -H^2G(\lambda_3(x,t)),\\ \lambda_{3t}(x,t) = g\lambda_2(x,t)+D(x)\left[\int_0^L D(x)\eta(x,t)\mathrm{d}x-\hat{\eta}(0,t)\right]+D\left(x-\dfrac{L}{\pi}\right)\left[\int_0^L D\left(x-\dfrac{L}{\pi}\right)\eta(x,t)\mathrm{d}x-\hat{\eta}\left(\dfrac{L}{\pi},t\right)\right],\\ \lambda_2(x,T) = \lambda_3(x,T) = 0,\end{cases} \tag{33}$$

where $G$ maps each $\lambda_3$ onto $\lambda_{1y}(x,0,t)$ defined by the solution of the following Laplace equation:

$$\begin{aligned}&\lambda_{1xx}(x,y,t)+H^2\lambda_{1yy}(x,y,t) = 0,\\ &\lambda_{1x}(0,y,t) = \lambda_{1x}(L,y,t) = 0,\\ &H^2\lambda_{1y}(x,-1,t) = 0,\\ &\lambda_1(x,0,t) = \frac{\lambda_3(x,t)}{H},\ \ G(\lambda_3)(x,t) = \lambda_{1y}(x,y,t)\big|_{y=0}.\end{aligned} \tag{34}$$

*Proof.* It follows from [23, Chapter 2] that the differential $\delta\mathcal{L}$ can be computed using the Lagrange approach as follows:

$$\delta\mathcal{L} = \frac{\mathrm{d}\mathcal{L}(\lambda+\epsilon\delta\lambda, p+\epsilon\delta p)}{\mathrm{d}\epsilon}\Big|_{\epsilon=0}, \tag{35}$$

where $\epsilon$ is a small real number variable producing small variation, which, added to the cost functional,

yields

$$\begin{aligned}\mathcal{L}(\lambda+\epsilon\delta\lambda,p+\epsilon\delta p)=&\frac{1}{2}\int_0^T\left[\int_0^L D(x)(\eta+\epsilon\delta\eta)\mathrm{d}x-\hat{\eta}(0,t)\right]^2\mathrm{d}t\\&+\frac{1}{2}\int_0^T\left[\int_0^L D\left(x-\frac{L}{\pi}\right)(\eta+\epsilon\delta\eta)\mathrm{d}x-\hat{\eta}\left(\frac{L}{\pi},t\right)\right]^2\mathrm{d}t\\&+\frac{1}{2}\int_0^L\left\{\epsilon_1[\xi^0(x)+\epsilon\delta\xi^0(x)-\xi_F^0(x)]^2+\epsilon_2[\eta^0(x)+\epsilon\delta\eta^0(x)-\eta_F^0(x)]^2\right\}\mathrm{d}x\\&+\int_0^T\int_0^L\int_{-1}^0(\lambda_1+\epsilon\delta\lambda_1)\left[\phi_{xx}+\epsilon\delta\phi_{xx}+(H+\epsilon\delta H)^2(\phi_{yy}+\epsilon\delta\phi_{yy})\right]\mathrm{d}y\mathrm{d}x\mathrm{d}t\\&+\int_0^T\int_0^L(\lambda_2+\epsilon\delta\lambda_2)\left[(\xi+\epsilon\delta\xi)_t+g(\eta+\epsilon\delta\eta)\right]\mathrm{d}x\mathrm{d}t\\&+\int_0^T\int_0^L(\lambda_3+\epsilon\delta\lambda_3)\left[(\eta+\epsilon\delta\eta)_t-(H+\epsilon\delta H)G(\xi+\epsilon\delta\xi)\right]\mathrm{d}x\mathrm{d}t.\end{aligned}\tag{36}$$

From (35), the differential $\delta\mathcal{L}$ is given as

$$\begin{aligned}\delta\mathcal{L}=&\int_0^T\int_0^L D(s)\left[\int_0^L D(x)\eta(x,t)\mathrm{d}x-\hat{\eta}(0,t)\right]\delta\eta\mathrm{d}s\mathrm{d}t\\&+\int_0^T\int_0^L D\left(s-\frac{L}{\pi}\right)\left[\int_0^L D\left(x-\frac{L}{\pi}\right)\eta(x,t)\mathrm{d}x-\hat{\eta}\left(\frac{L}{\pi},t\right)\right]\delta\eta\mathrm{d}s\mathrm{d}t\\&+\int_0^L\left\{\epsilon_1(\xi^0-\xi_F^0)\delta\xi^0+\epsilon_2(\eta^0-\eta_F^0)\delta\eta^0\right\}\mathrm{d}x\\&+\int_0^T\int_0^L\int_{-1}^0\lambda_1(\delta\phi_{xx}+2H\phi_{yy}\delta H+H^2\delta\phi_{yy})\mathrm{d}y\mathrm{d}x\mathrm{d}t\\&+\int_0^T\int_0^L\lambda_2(\delta\xi_t+g\delta\eta)\mathrm{d}x\mathrm{d}t\\&+\int_0^T\int_0^L\lambda_3[\delta\eta_t-G(\xi)\delta H-H\delta G(\xi)]\mathrm{d}x\mathrm{d}t,\end{aligned}\tag{37}$$

where the relations $\phi_{xx}+H^2\phi_{yy}=0$, $\xi_t+g\eta=0$, and $\eta_t-HG(\xi)=0$ have been utilized. Using integration by parts, it yields

$$\begin{aligned}\int_0^T\lambda_2\delta\xi_t\mathrm{d}t&=[\lambda_2\delta\xi]_{t=0}^T-\int_0^T\lambda_{2t}\delta\xi\mathrm{d}t,\\\int_0^T\lambda_3\delta\eta_t\mathrm{d}t&=[\lambda_3\delta\eta]_{t=0}^T-\int_0^T\lambda_{3t}\delta\eta\mathrm{d}t,\\\int_0^L\int_{-1}^0\lambda_1(\delta\phi_{xx}+H^2\delta\phi_{yy})\mathrm{d}y\mathrm{d}x=&-\int_{-1}^0[\lambda_{1x}\delta\phi]_{x=0}^L dy+\int_0^L\left\{[H^2\lambda_1\delta\phi_y]_{y=0}-[H^2\lambda_{1y}\delta\phi]_{y=-1}^0\right\}\mathrm{d}x\\&+\int_0^L\int_{-1}^0(\lambda_{1xx}+H^2\lambda_{1yy})\delta\phi\mathrm{d}y\mathrm{d}x,\end{aligned}\tag{38}$$

where the constraint conditions $\delta\phi_x|_{x=0}=\delta\phi_x|_{x=L}=\delta\phi_y|_{y=-1}=0$ have been utilized. Therefore, we

obtain

$$\begin{aligned}\delta\mathcal{L}=&\int_0^T\int_0^L D(s)\left[\int_0^L D(x)\eta(x,t)\mathrm{d}x-\hat{\eta}(0,t)\right]\delta\eta\mathrm{d}s\mathrm{d}t\\&+\int_0^T\int_0^L D\left(s-\frac{L}{\pi}\right)\left[\int_0^L D\left(x-\frac{L}{\pi}\right)\eta(x,t)\mathrm{d}x-\hat{\eta}\left(\frac{L}{\pi},t\right)\right]\delta\eta\mathrm{d}s\mathrm{d}t\\&+\int_0^L\left[\epsilon_1(\xi^0-\xi_F^0)\delta\xi^0+\epsilon_2(\eta^0-\eta_F^0)\delta\eta^0\right]\mathrm{d}x\\&+\int_0^T\int_0^L\int_{-1}^0(\lambda_{1xx}+H^2\lambda_{1yy})\delta\phi+2H\lambda_1\phi_{1yy}\delta H\ \mathrm{d}y\mathrm{d}x\mathrm{d}t\\&+\int_0^T\int_0^L\left\{[H^2\lambda_1\delta\phi_y]_{y=0}-[H^2\lambda_{1y}\delta\phi]_{y=-1}^0\right\}\mathrm{d}x\mathrm{d}t-\int_0^T\int_{-1}^0[\lambda_{1x}\delta\phi]_{x=0}^L\mathrm{d}y\mathrm{d}t+\int_0^L[\lambda_2\delta\xi]_{t=0}^T\mathrm{d}x\\&+\int_0^T\int_0^L\left[-\lambda_{2t}\delta\xi+g\lambda_2\delta\eta\right]\mathrm{d}x\mathrm{d}t+\int_0^L[\lambda_3\delta\eta]_{t=0}^T\mathrm{d}x\\&-\int_0^T\int_0^L\left\{\lambda_{3t}\delta\eta+\lambda_3[G(\xi)\delta H+H\delta G(\xi)]\right\}\mathrm{d}x\mathrm{d}t.\end{aligned}\tag{39}$$

The idea of constructing an adjoint equation is to obtain the differential of $\mathcal{L}$ with respect to parameter variation. Therefore, we implement the factor of other variations to be equal to zero. In other words, making the factor of $\delta\phi,\delta\phi|_{x=0},\delta\phi|_{x=L},\delta\phi|_{y=-1}$, and $\delta\phi_y|_{y=0}$ to be equal to zero leads to

$$\begin{cases}\lambda_{1xx}(x,y,t)+H^2\lambda_{1yy}(x,y,t)=0,\\ \lambda_{1x}(0,y,t)=\lambda_{1x}(L,y,t)=0,\\ \lambda_{1y}(x,-1,t)=0,\\ \lambda_1(x,0,t)=\dfrac{\lambda_3(x,t)}{H}.\end{cases}\tag{40}$$

Imposing the factor of $\delta\eta$ and $\delta\xi$ to be zero leads to

$$\begin{aligned}&\lambda_{3t}(x,t)=g\lambda_2(x,t)+D(x)\left[\int_0^L D(x)\eta(x,t)\mathrm{d}x-\hat{\eta}(0,t)\right]+D\left(x-\frac{L}{\pi}\right)\left[\int_0^L D\left(x-\frac{L}{\pi}\right)\eta(x,t)\mathrm{d}x-\hat{\eta}\left(\frac{L}{\pi},t\right)\right],\\&\lambda_{2t}(x,t)=-H^2G(\lambda_3(x,t)).\end{aligned}\tag{41}$$

Ensure that the factors of $\delta\xi|_{t=T}$ and $\delta\eta|_{t=T}$ to be zero are equivalent to

$$\lambda_2(x,T)=0,\quad \lambda_3(x,T)=0.\tag{42}$$

After substituting (40)–(42) into (39), the differential of $\mathcal{L}$ can be written as

$$\delta\mathcal{L}=\left\langle \mathrm{d}\mathcal{L},\begin{bmatrix}\delta H\\ \delta\xi^0\\ \delta\eta^0\end{bmatrix}\right\rangle,\tag{43}$$

where $\mathrm{d}\mathcal{L}$ is the derivative of $\mathcal{L}$ as defined in (32). The proof of Theorem 2 is complete.

**Remark 3.** We state that the adjoint system (33) and (34) represents an LWWE backward in time.

Once the cost functional derivative is available, we can use the gradient descent technique to find a local minimum of the cost functional. The identification algorithm is designed as follows:

(1) Guess a suitable solution $\xi_F^0(x)$ and $\eta_F^0(x)$.
(2) Set an initial value for simulation $(H_0,\xi_0^0,\eta_0^0)$ and initialize a counter $k=0$.
(3) Test the stop condition, i.e., $|J|<\epsilon$, and stop the algorithm.
(4) Simulation forward in time from $t=0$ to $T$ the system model (26) and (27) with $(H_0,\xi_0^0,\eta_0^0)$.
(5) Simulation backward in time from $t=T$ to 0 the adjoint model (33) and (34).

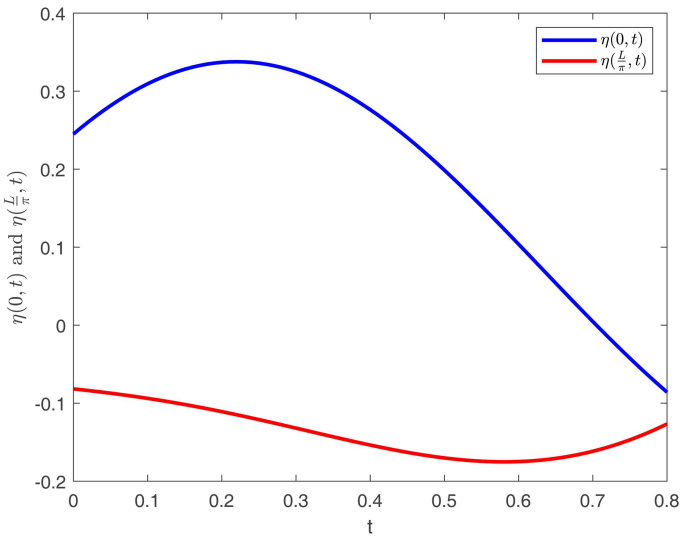


**Figure 2** (Color online) Measurement records $\eta(x,t)$.

(6) Compute the derivative $d\mathcal{L}$ by using (32). To get the image of $[g\epsilon_1(\xi^0-\xi_F^0)-g\lambda_1(x,0)]$ under the mapping $G^{-1}$, the Laplace equation (10) is solved, and the solution is evaluated on $y=0$.

(7) Use the GDM to update the new value of $(H,\xi^0,\eta^0)$ at iteration $k+1$,

$$\begin{aligned} H_{k+1} &= H_k - a_k\frac{\partial\mathcal{L}}{\partial H_k},\\ \xi_{k+1}^0 &= \xi_k^0 - b_k\frac{\partial\mathcal{L}}{\partial\xi_k^0},\\ \eta_{k+1}^0 &= \eta_k^0 - c_k\frac{\partial\mathcal{L}}{\partial\eta_k^0}, \end{aligned} \tag{44}$$

where $a_k$, $b_k$, and $c_k$ are positive real numbers that were chosen properly for the three step sizes in iterations, respectively.

(8) Put $k=k+1$ and return to step (3).

## 5 Numerical simulations

We use the MATLAB software to test the identification algorithm. We assume that the length of the container is $L=3$ m and the gravitational acceleration constant is $g=9.8$ m/s$^2$. The real values of the initial condition and water depth are supposed to be

$$\begin{aligned} \xi^0(x) &= \sqrt{\frac{2}{L}}\sqrt{\frac{g}{k_1\tanh(k_1h)}}0.2\cos(k_1x)+\sqrt{\frac{2}{L}}\sqrt{\frac{g}{k_2\tanh(k_2h)}}0.1\cos(k_2x),\\ \eta^0(x) &= \sqrt{\frac{2}{L}}0.2\cos(k_1x)+\sqrt{\frac{2}{L}}0.1\cos(k_2x),\\ H &= 1, \end{aligned} \tag{45}$$

where $k_1=\pi/L$ and $k_2=2\pi/L$. In this section, we use the finite difference method to compute the numerical solution of the LWWE (1)–(3). $\Delta x=0.3$ m, $\Delta y=0.1$ m, and $\Delta t=0.01$ s are the spatial and temporal grid densities selected for the finite difference method. We refer to [11] for the detailed presentation of the finite difference scheme of the LWWE. After simulation of 0.8 s, we present the measurement data of water wave elevation, i.e., $\eta(0,t)$ and $\eta\left(\frac{L}{\pi},t\right)$, in Figure 2.

### 5.1 Simulation result of two-point wave elevation measurement

In the first simulation, we extract the wave elevation records at position $x=0$ and $x=\frac{L}{\pi}$ with only 80 discrete time samples as the measurement data to the system. The initial values that are fed to the

**Table 1** Relationship between the step size and the number of iterations

| Step size | Iteration number | Step size | Iteration number | Step size | Iteration number |
|---|---|---|---|---|---|
| 0.1 | 2973 | 0.9 | 328 | 1.7 | 172 |
| 0.3 | 989 | 1.1 | 268 | 1.9 | 153 |
| 0.5 | 592 | 1.3 | 226 | 2.1 | 138 |
| 0.7 | 422 | 1.5 | 195 | | |

identification algorithm are

$$\begin{aligned} &\xi_0^0(x) = \eta_0^0(x) = \sqrt{\frac{2}{L}}\cos(k_1 x), \\ &d_0 = 2 \text{ m}. \end{aligned} \tag{46}$$

The calibration coefficients are chosen as $\epsilon_1 = \epsilon_2 = 1 \times 10^{-7}$. The first guessed value of the initial condition is set to zero. We choose a fixed step size for the algorithm in the iterations. Moreover, the Delta-Dirac function $D(x)$ is approximated by a Gaussian function $D(x) = \frac{2}{\sigma\sqrt{\pi}}\mathrm{e}^{-x^2/\sigma^2}$ with a small variance $\sigma = 0.01$.

Table 1 lists the number of iterations required to achieve the same target functional $\min \mathcal{L} = 2.97 \times 10^{-5}$ with different iteration steps. From Table 1, one may misunderstand that a larger iteration step size requires a fewer number of iterations. However, we found that the algorithm diverged as we continued to increase the iteration step size. Moreover, we found that the range of iteration step size for the algorithm is from 0.1 to 2.1.

After multiple simulations, we found that the optimal step sizes are $a = 0.1$, $b = 0.3$, and $c = 1$, where $a$, $b$, and $c$ are the step sizes corresponding to $\xi^0$, $\eta^0$, and $h$, respectively. After 137 iterations, we found that the minimum value of cost functional is $\min \mathcal{L} = 2.97 \times 10^{-5}$, and the optimal water depth value is 1.0017 m. Figure 3(a) shows the evolution of the estimated water depth, where the red line and the dashed line (in blue) are the true value $H = 1$ m and the estimated water depth, respectively. The relative error between the real water depth value and the estimated one is 0.17%, which is quite small. Furthermore, one can observe the estimation results for $\xi^0(x)$ in Figure 3(b). As shown in Figure 3(b), the estimation of velocity potential converges to the real values with some small bias around $x = 1.5$ m. Figure 3(c) shows the estimated results for $\eta^0(x)$, revealing that the estimation accuracy of the algorithm for $\eta^0(x)$ is more satisfactory than that of $\xi^0(x)$.

### 5.2 Simulation result of distributed measurement of wave elevation

In this subsection, we assume that the distributed water wave elevation is measurable and available to design the identification algorithm. The purpose of this group of simulations is to show the advantage of the adjoint method by comparing the method with the existing work [13]. To estimate the water depth and velocity potential, we replace the cost functional in (29) by

$$J = \frac{1}{2}\int_0^T \int_0^L [\eta(x,t) - \hat{\eta}(x,t)]^2 \mathrm{d}x\mathrm{d}t + \frac{1}{2}\epsilon_1 \int_0^L [\xi^0(x) - \xi_F^0(x)]^2 \mathrm{d}x. \tag{47}$$

From the procedure of the proof of Theorem 2, we find that the corresponding adjoint equations are

$$\begin{aligned} &\lambda_{2t}(x,t) = -d^2 G(\lambda_3(x,t)), \\ &\lambda_{3t}(x,t) = g\lambda_2(x,t) + [\eta(x,t) - \hat{\eta}(x,t)], \\ &\lambda_2(x,T) = \lambda_3(x,T) = 0, \end{aligned} \tag{48}$$

where $G$ has the same definition as that of (33).

The initial values fed to the estimation algorithm are $\xi_0^0(x) = 0$ and $H_0 = 2$ m. The calibration coefficient is chosen as $\epsilon_1 = 1 \times 10^{-7}$.

After 131 iterations, we found that the minimum value of cost functional is $\min \mathcal{L} = 7.71 \times 10^{-6}$, and the optimal water depth value is 0.997 m. Figure 4(a) shows the evolution of the estimated water depth, where the blue line and the dashed line (in red) are the actual value $H = 1$ m and the estimated water depth, respectively. The relative error between the actual water depth value and the estimated one is 0.3%, which is quite small. Furthermore, one can observe the estimation results for $\xi^0(x)$ in Figure 4(b). We find that water depth estimation is similar by comparing the simulation results of two-point observation and

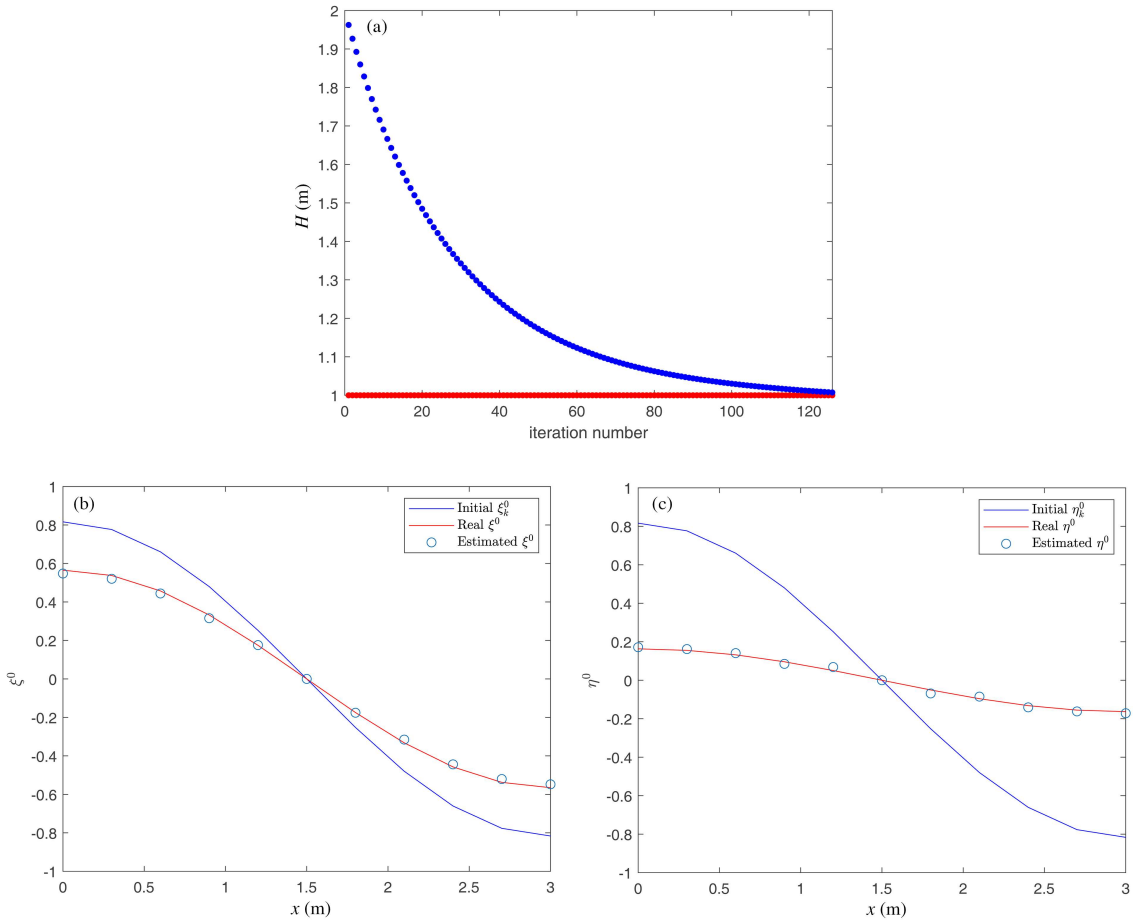


**Figure 3** (Color online) (a) Evolution of water depth with point measurement; (b) estimation of $\xi^0(x)$ with point measurement; (c) estimation of $\eta^0(x)$ with point measurement.

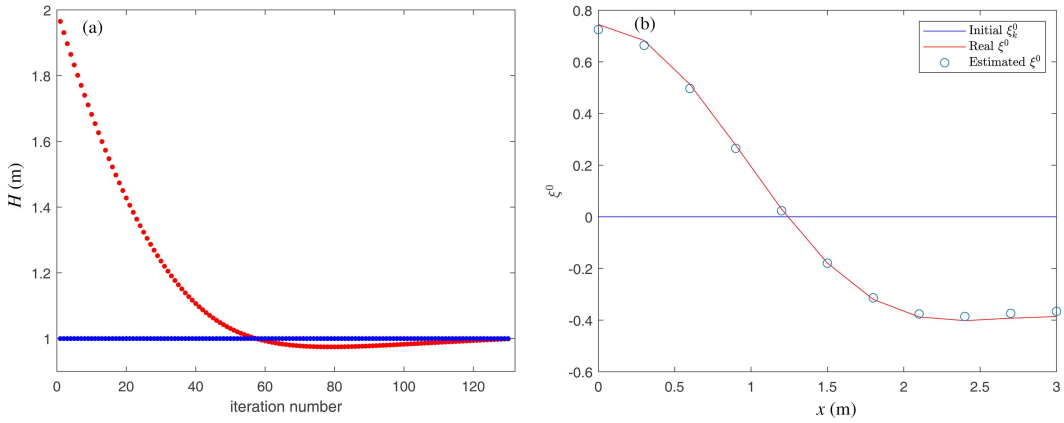


**Figure 4** (Color online) (a) Evolution of water depth with distributed measurement; (b) estimation of $\xi^0(x)$ with distributed measurement.

distributed observation. The identification accuracy of $\xi^0$ caused by distributed observation is better than that of two-point observation. From an application perspective, point observations in infinite-dimensional systems are more economical than distributed observations.

Compared with the existing studies [13], the advantages of the adjoint method include the following two aspects. First, the adjoint method does not rely on the analytical solution of the system model. Ref. [13] first obtained the analytical solution of the LWWE and then used the analytical solution as the model of water waves to identify the water depth and velocity potential. However, the designed

adjoint method directly uses the mathematical model of the dynamical system to determine the direction of reducing the cost functional by constructing the adjoint equation of the system. Second, the adjoint method converges faster than that of [13]. Under the same initial conditions and observation output, the adjoint method only requires 131 iterations to drive the cost functional to $7.71 \times 10^{-6}$. However, the classical gradient method used in [13] requires 270 iterations for the exact identification accuracy.

## 6 Conclusion and future perspectives

In this paper, we study the identification problem of water depth and state variables of the LWWE. Based on the adjoint method, we have designed an identification algorithm that can simultaneously estimate the state and parameters of water waves. Numerical simulations allowed us to test the performance of the designed identification algorithm. Moreover, numerical simulations show that the two-point wave elevation measurement makes it possible to reconstruct the water depth and the state trajectories of water waves.

Our future work will focus on actual experiments in the sea area near Qingdao, China, and will use the mapping data to investigate the practicability of the identification algorithm.

**Acknowledgements** This work was partially supported by National Natural Science Foundation of China (Grant Nos. 61973179, 62403263), Natural Science Foundation of Qingdao, China (Grant No. 24-4-4-zrjj-88-jch), Foundation of Key Laboratory of Autonomous Systems and Networked Control (South China University of Technology), Ministry of Education (Grant No. 2014A01), and French Grant ANR ODISSE (Grant No. ANR-19-CE48-0004-01). The authors would like to thank anonymous reviewers for their constructive comments which helped improve the quality and presentation of this paper.

**References**

1 Dean R G, Dalrymple R A. Water Wave Mechanics for Engineers and Scientists. Singapore: World Scientific Publishing Co. Inc., 1991
2 Whitham G B. Linear and Nonlinear Waves, volume 42. Hoboken: John Wiley & Sons, 2011
3 Lannes D. The Water Waves Problem: Mathematical Analysis and Asymptotics. Providence: American Mathematical Society, 2013
4 Nouguier F, Grilli S T, Guerin C A. Nonlinear ocean wave reconstruction algorithms based on simulated spatiotemporal data acquired by a flash LIDAR camera. IEEE Trans Geosci Remote Sens, 2014, 52: 1761–1771
5 Fontelos M A, Lecaros R, López J C, et al. Bottom detection through surface measurements on water waves. SIAM J Control Optim, 2017, 55: 3890–3907
6 Vasan V, Deconinck B. The inverse water wave problem of bathymetry detection. J Fluid Mech, 2013, 714: 562–590
7 Reid R M, Russell D L. Boundary control and stability of linear water waves. SIAM J Control Optim, 1985, 23: 111–121
8 Mottelet S. Controllability and stabilization of a canal with wave generators. SIAM J Control Optim, 2000, 38: 711–735
9 Su P, Tucsnak M, Weiss G. Stabilizability properties of a linearized water waves system. Syst Control Lett, 2020, 139: 104672
10 Alazard T. Boundary observability of gravity water waves. Ann Inst H Poincaré Anal Non Linéaire, 2018, 35: 751–779
11 Yu Y, Pei H-L, Xu C-Z. Estimation of velocity potential of water waves using a Luenberger-like observer. Sci China Inf Sci, 2020, 63: 222201
12 Yu Y, Xu C-Z, Yu J. Design of infinite-dimensional observers for a linearized water wave system with distributed or point measurement. IEEE Trans Automat Contr, 2024, 69: 2729–2736
13 Yu Y, Pei H-L, Xu C-Z. Identification of water depth and velocity potential for water waves. Syst Control Lett, 2019, 125: 29–36
14 Nguyen V T, Georges D, Besançon G. Optimal state estimation in an overland flow model using the adjoint method. In: Proceedings of IEEE Conference on Control Applications (CCA), 2014. 2034–2039
15 Roman C, Ferrante F, Prieur C. Parameter identification of a linear wave equation from experimental boundary data. IEEE Trans Contr Syst Technol, 2021, 29: 2166–2179
16 Nguyen V T, Georges D, Besançon G. Calculus of variations approach for state and parameter estimation in switched 1D hyperbolic PDEs. Optim Control Appl Methods, 2018, 39: 1182–1201
17 Ruder S. An overview of gradient descent optimization algorithms. 2016. ArXiv:1609.04747
18 Zhou H-C, Guo B-Z. Unknown input observer design and output feedback stabilization for multi-dimensional wave equation with boundary control matched uncertainty. J Differ Equ, 2017, 263: 2213–2246
19 Zhou H-C, Guo B-Z, Xiang S-H. Performance output tracking for multidimensional heat equation subject to unmatched disturbance and noncollocated control. IEEE Trans Automat Contr, 2020, 65: 1940–1955
20 Craig W, Sulem C. Numerical simulation of gravity waves. J Comput Phys, 1993, 108: 73–83
21 Zakharov V E. Stability of periodic waves of finite amplitude on the surface of a deep fluid. J Appl Mech Tech Phys, 1972, 9: 190–194
22 Blenkinsopp C E, Mole M A, Turner I L, et al. Measurements of the time-varying free-surface profile across the swash zone obtained using an industrial LIDAR. Coast Eng, 2010, 57: 1059–1065
23 Kot M. A First Course in the Calculus of Variations. Providence: AMS, 2014